J Nanostruct 6(3): 221-234, Summer 2016

RESEARCH PAPER

Fabrication and Evaluation of Pt/M (M= Co, Fe) Chitosan Supported Catalysts for Methanol Electrooxidation: Application in Direct Alcohol Fuel Cell

Mehri-Saddat Ekrami-Kakhki[1], Zahra Yavari[2], Jilla Saffari[3] and Sedigheh Abbasi[1]*

[1] *Esfarayen University of Technology, Esfarayen, North Khorasan, Iran*

[2] *Department of Chemistry, University of Sistan and Baluchestan, Zahedan, Iran*

[3] *Department of Chemistry, Zahedan Branch, Islamic Azad University, Zahedan, Iran.*

ARTICLE INFO

Article History:
Received 28 April 2016
Accepted 10 June 2016
Published 1 July 2016

Keywords:
Chitosan
Direct methanol fuel cell
Fuel cell
Methanol electrooxidation
Nanoparticles

ABSTRACT

In this work, Pt, Fe and Co nanoparticles were prepared by chemical reduction of the metal salts in chitosan as the support. $NaBH_4$ was used as the reducing agent Pt-Fe, Pt-Co and Pt-Fe-Co-chitosan nanocomposites were synthesized and characterized by UV–Vis spectra and Transmission electron microscopy images. GC/Pt-chitosan, GC/Pt-Co-chitosan, GC/Pt-Fe-chitosan and GC/Pt-Co-Fe-chitosan electrodes were prepared. The performances of these electrodes for methanol electrooxidation were investigated through cyclic voltammetric and chronoamperometric curves. The effect of some experimental factors such as the amounts of Fe and Co nanoparticles dispersed in chitosan, methanol concentration and scan rate were studied and the optimum conditions were determined. The effect of temperature was also investigated and the activation energies were calculated. The performance of Pt-Fe-Co-chitosan nanocomposites was determined in a direct methanol fuel cell in different conditions. The electrochemical and fuel cell measurements showed that Pt-Fe-Co-chitosan nanocatalyst has the best activity for electrooxidation of methanol among all different compositions electrodes.

How to cite this article
Ekrami-Kakhki M, Yavari Z, Saffari J, Abbasi S. Fabrication and Evaluation of Pt/M (M= Co, Fe) Chitosan Supported Catalysts for Methanol Electrooxidation: Application in Direct Alcohol Fuel Cell. J Nanostruct, 2016; 6(3):221-234. DOI: 10.7508/JNS.2016.03.007

INTRODUCTION

In response to increasing energy needs and emerging ecological concerns in the world, energy should be produced as much as possible in an environmentally friendly manner. Particular focus is on fuel cells, which can produce the electrical power directly from the chemical energy with high efficiency and zero emission of pollutants [1]. Among all types of the fuel cells, a great attention is attracted on direct methanol fuel cells (DMFCs) which have interesting applications in transportation part and portable electronic devices. This happens since liquid methanol fuels has higher energy density than gaseous fuels like hydrogen [2], rapid response to catalyst loading, quick start-up, high energy density and lower operating temperatures besides least emission of pollutants [3]. Pt is the best catalyst for methanol oxidation (MO) in acidic media, but it is a precious and very expensive metal and its surface is easily poisoned by the adsorbed carbonaceous species such as CO produced during the anodic process of methanol dehydrogenation. Poisoning of the Pt surface inhibits further adsorption of the methanol molecules [4]. To avoid surface poisoning and also to improve the catalytic activity of the platinum catalysts, addition of other elements has been widely investigated

* *Corresponding Author Email: Ekrami@Esfarayen.ac.ir*

[5]. Bimetallic nanoalloys Pt–M (M= Ni, Fe, Co, Pd, Cr, Au, and Ru) have shown higher catalytic activity and durability for MO reaction than Pt nanoparticles [6–8]. Alloying of Pt with secondary metal reduces its CO poisoning effect and also makes it cheaper [6]. Pt–Ru nanoalloys have shown better efficiency than Pt nanoparticles but they are more expensive and are undesirable for industrial applications due to their toxicological effect [9]. Pt–Cu nanocube catalysts have been prepared through a colloidal approach [10]. Pt–Sn bimetallic catalyst has been synthesized via the electrochemical deposition process [11]. Pt–SiO_2 nanocomposite has been prepared by Salabat et al. [12]. Among many synthesized bimetallic nanocatalysts, preparation of Fe-Pt alloys are on the focus. For example, Fe-Pt nanoparticles have been prepared on reduced graphene oxide (RGO) [13]. Many polymers, such as nafion, polyaniline and chitosan (CH) have been used as support for metal nanoparticles. Chitosan is a polysaccharide biopolymer obtained from naturally occurring chitin. It has interesting chelating, film-forming and polycationic properties. It can be used as the support for the catalysts. These properties are attained because of the active hydroxyl and amino functional groups in its structure. Chitosan membranes have also shown very good performance in low temperature fuel cells [14]. Recently, synthesis of chitosan-based metal nanomaterials has attracted increasing attention. Unique bioactivity, conformation and flexibility of this polymer made it a good support for catalysts and particularly heterogeneous catalysts [15].

In this study, Multifunctional nanocatalysts, PtNPs, PtNPs–CoNPs, PtNPs-FeNPs and PtNPs-CoNPs-FeNPs dispersed in chitosan, were successfully synthesized and their catalytic activity toward MO reaction was compared with each others. The effect of some experimental factors on the potential and anodic current density of MO was studied and the optimum conditions were determined. The catalytic activity of as-prepared electrodes for MO was also investigated in different temperatures and the kinetic investigation has been done. Finally, the functions of PtNPs–CoNPs-FeNPs-CH nanocomposites were investigated in stack and assembled DMFC as anodic catalysts. The fuel cell polarization curves were plotted for mentioned DMFC.

MATERIALS AND METHODS

H_2PtCl_6, cobalt chloride and iron chloride were purchased from Merck and used as metal precursor. Sulfuric acid and $NaBH_4$ were used as the electrolyte and reducing agent, respectively and purchased from Merck. Chitosan ([2-amino-2-deoxy-(1-4)-β-D-glucopyranose]), with medium molecular weight, 400000 Da, was obtained from Fluka. Chitosan solution was prepared by dissolving of chitosan in 1% aqueous solution of acetic acid supplied by Merck. All solutions were prepared by doubly distilled water. Nitrogen bubbling was used to deoxygenate the electrolyte solutions before each voltammetric experiment. Deagglomerated alumina powder 0.05 µm was used for polishing of the glassy carbon (GC) working electrode. Analytical grade methanol from Merck was use to investigate MO. TEM images were taken using a Philips CM120 transmission electron microscope with the resolution 2.5 Å. UV-Vis spectra were obtained on an analytikjena SPE-CORD S100 spectrometer with photodiode array detector. Electrochemical measurements were used to investigate the catalytic activity of the prepared nanocomposites. A potentiostat/galvanostat Autolab (Nova software model PGSTAT 302N, Metrohm, Netherlands) and a conventional three-electrode cell was used. A saturated calomel electrode (SCE) was used as the reference electrode. A platinum electrode and the glassy carbon electrode (2 mm of diameter) were used as the auxiliary and working electrode, respectively. All the experiments were done at scan rate of 100 m Vs^{-1}. The electrolyte solutions made of 30 ml of 0.5 M H_2SO_4 or 0.5 M H_2SO_4.

Preparation of metal-chitosan nanocomposites

Since methanol electrooxidation was studied at the glassy carbon electrodes covered by a thin film of chitosan incorporated platinum, cobalt, iron, platinum-cobalt, platinum-iron and Platinum-cobalt-iron nanoparticles, so preparation of the nanoparticles should be investigated initially. At first, chitosan solution (2 mg/ml) was prepared in 1% acetic acid solution. Because of the poor solubility of chitosan, it was stirred until the entire dissolution and kept for overnight. In order to remove any impurity from the chitosan solution, it was finally filtrated through 0.22 m Millipore syringe filters. The general approach for the

synthesis of the Fe and Co modified supported Pt catalysts and production of the metal nanoparticles was chemical reduction of the appropriate metal salts with $NaBH_4$ as the reducing agent. To get the entire reduction, the concentration of $NaBH_4$ was selected 10 times of the metal salt. In a typical procedure, a 25 µl metal salts ($CoCl_2$. $6H_2O$ (0.04 M), $FeCl_3.6H_2O$ (0.04 M) and H_2PtCl_6 (1M) or a mixture of metal salts aqueous solution) was mixed with 3 ml of chitosan solution, the mixtures were stirred using a rotary aperture (100 rpm) for 90 min, then freshly prepared aqueous solutions of $NaBH_4$ (50µl, 0.4M) were added to the mixture, and stirred for another 30 min until the entire reduction of metal salts The resulted nanocomposites were kept at room temperature for characterization.

Preparation of the electrodes

Before each electrochemical experiment, the GC electrode was polished with 0.05 µm alumina slurry and sonicated in water and absolute ethanol. It was cleaned and activated by cyclic voltammetry between −1.5 and +1.5 V in freshly prepared deoxygenated 1.0 mol L^{-1} H_2SO_4 then was used as the substrate for catalyst. 5 µl of the prepared nanocomposites was deposited onto a GC electrode. The subsequent evaporation of solvent at room temperature led to the formation of the deposited catalyst layer.

RESULTS AND DISCUSSION

Characterization data of some important Compounds

The formation of metal nanoparticles was confirmed by TEM images and UV–Vis spectra. Fig. 1 showed the UV–Vis spectra of platinum, cobalt and iron–chitosan nanocomposites with the same concentration of metal ions as precursor. For platinum nanoparticles, no plasmon absorbance could be seen between 300 and 600 nm and this result is consistent with that reported by Yang et al. [16]. The absorption spectrum of Pt(IV) species was observed at 265 nm (Fig. 1A (a)) [17]. It disappeared completely after the reaction, indicating that Pt(IV) had been used up and colloidal Pt had been formed (Fig. 1A (b)). UV-Vis spectra of $CoCl_2$ solution and Co nanoparticles was seen in Fig. 1B. As observed there is not any absorption peak for $CoCl_2$ solution in the range of

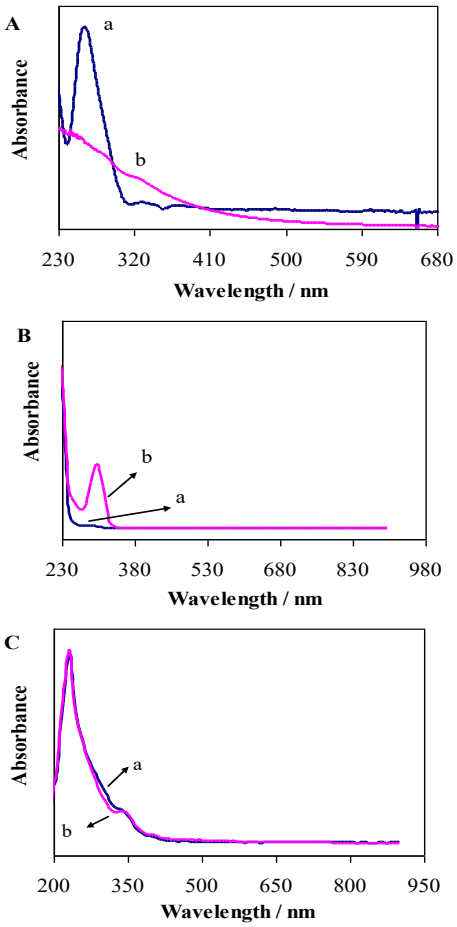

Fig. 1. UV–Vis absorption spectra of A (a) H_2PtCl_6 solution, A (b) Pt nanoparticles, B (a) $CoCl_2$ solution, B (b) Co nanoparticles, C (a) $FeCl_2$ solution and C (b) Fe nanoparticles dispersed in chitosan.

230 nm to 890 nm (Fig. 1B (a)). Fig. 1B (b) showed UV-Vis absorption spectra of Co nanoparticles dispersed in chitosan. The absorption peak of the spectrum at 300 nm was attributed to the formation of cobalt nanoparticles [18]. Formations of Iron nanoparticles were detected by UV-Vis spectrum shown at Fig. 1C (b). Absorptions peaks of the spectrum were observed at two wavelengths (230 nm and 340 nm). The shifts in peaks of nanoparticles may be due to media compositions or size of particles [19].

UV-Vis spectrum of $FeCl_2$ solution was shown at Fig. 1C (a).

Fig. 2 showed TEM images of platinum, platinum-cobalt and platinum-iron nanoparticles dispersed in chitosan. It was observed from TEM images that nanoparticles were successfully synthesized. The overall particle size of the nanoparticles ranged

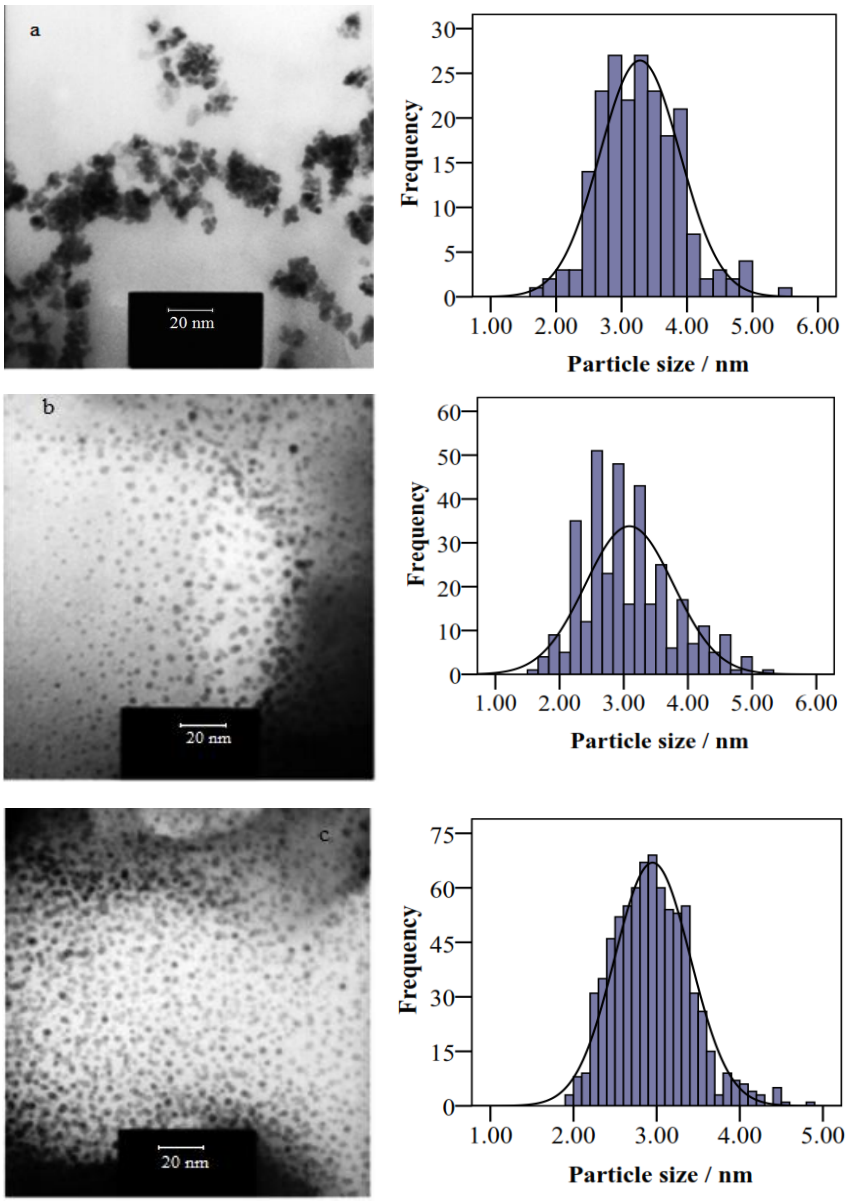

Fig. 2. TEM images of (a) platinum, (b) platinum-cobalt, and (c) platinum-iron nanoparticles distributed in chitosan

around 2 to 4 nm and that particles exhibited fine spherical features and good dispersion in chitosan.

Electrochemical characterization

The electrochemical surface area (EAS) of PtNPs is an important factor for the determination of catalytic activity, especially for an oxidation reaction as a surface reaction. This parameter can be calculated by cyclic voltammetry techniques. The voltammogram of H_2 adsorption/desorption was used to determine EAS amount of the modified electrodes (Fig. 3B). The columbic charge (Q_H) for hydrogen adsorption/desorption was employed for calculation the platinum EAS of the modified electrodes. The Q_H value is considered as the mean value between the amounts of charge exchanged during the electrochemically adsorption (Q''_H) and desorption (Q'_H) of H_2 on PtNPs sites [20] (eq. 1).

$$Q_H = (Q'_H+Q''_H)/2 \quad (1)$$

It was calculated by measuring the area under

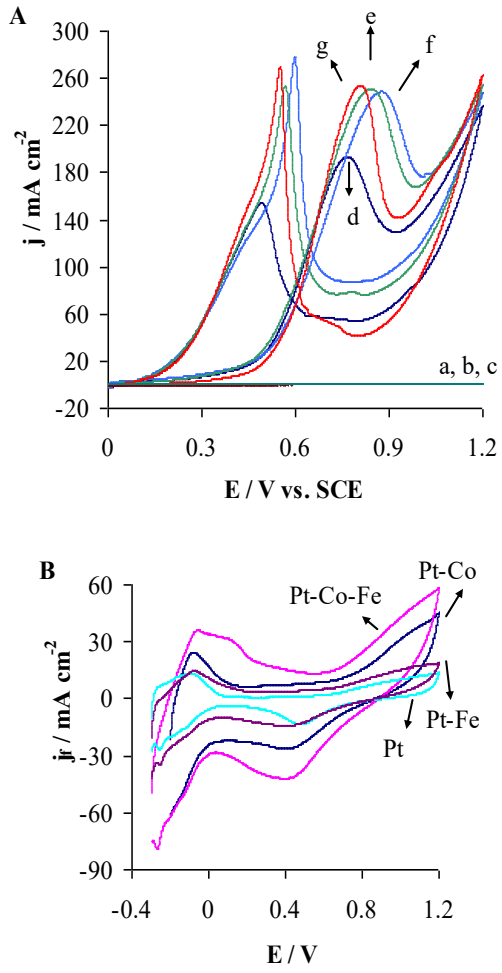

Fig. 3. A) CVs for MO in 1.5 M methanol and 0.5 M H2SO4 at a) GC/CH, b) GC/CoNPs-CH, c) GC/FeNPs-CH, d) GC/Pt-NPs-CH, e) GC/PtNPs-FeNPs-CH, f) GC/PtNPs-CoNPs-CH and g) GC/PtNPs-CoNPs-FeNPs-CH electrodes. B) Cyclic voltammograms of as-prepared electrodes in 0.5 M H_2SO_4

the peak at potential rang of hydrogen adsorption/desorption on modified electrodes. The EAS amount for PtNPs was calculated electrochemically using Q_H and equation (2) [21].

$$EAS=Q_H/S\times L \quad (2)$$

Where L is the PtNPs loading (mg.cm^{-2}) that was 0.51 mg.cm^{-2} for the modified electrodes and S is a parameter relating the charge to area (=0.21 mC.m^{-2}). This represents the charge required for the oxidation of a H_2 adsorbed monolayer on Pt particles. Table 1 showed the calculated EAS on modified electrodes with similar PtNPs loading.

As seen in table 1, EAS amount of as-prepared nanocatalysts was as follows:

PtNPs-CH<PtNPs-FeNPs-CH<PtNPs-CoNPs-CH<PtNPs-CoNPs-FeNPs-CH

EAS amount of PtNPs-CoNPs-FeNPs-CH nanocatalyst was higher than other prepared catalysts showing that this catalyst had higher catalytic activity for MO reaction.

Methanol oxidation reaction (MOR)

Electrochemical characteristics of the modified electrodes have been determined by cyclic voltammetry in 0.5 M H_2SO_4 and 1.5 M CH_3OH solution and the obtained cyclic voltammograms for GC/CH, GC/CoNPs-CH, GC/FeNPs-CH, GC/PtNPs-CH, GC/PtNPs-CoNPs-CH, GC/PtNPs-FeNPs-CH and GC/PtNPs-CoNPs-FeNPs-CH nanocomposites were shown in Fig. 3. No current peaks of MO was seen in the CV curves of the GC and GC/CH electrodes (Fig. 3a), which indicates that the GC and GC/CH substrate has no obvious electrocatalytic activity for MO (CV at GC electrode was not shown, which was similar to that of GC/CH electrode). Cyclic voltammograms of GC/CoNPs-CH and GC/FeNPs-CH electrodes were shown in Fig. 3b and 3c. As observed, these electrodes had no obvious electrocatalytic activity for MO. On the other hand, the typical cyclic voltammogram for MO in 0.5 M H_2SO_4 obtained with a GC/CH electrode containing the PtNPs dispersed electrocatalyst (GC/PtNPs-CH) was presented in the Fig. 3d and high electrocatalytic activity was observed.

The portion of the surface available in dispersion of the metallic particles determines the electrocatalytic activity of the electrode. It has been reported that a better dispersion of the nanoparticles could be obtained by using a more porous matrix of the conductive polymers with a larger portion of the surface which prevents agglomeration of the metallic particles [22]. As observed in Fig. 3d, two peaks of MO can be seen obviously in the range of 0.0 to 1.2 V for GC/PtNPs-CH. Two oxidation peaks can be seen obviously at 0.767 (E_f) and 0.487 V (E_b), respectively. The

Table 1. The EAS amount of the modified electrodes with the platinum loading 0.51 mg.cm^{-2} in 0.5 M H_2SO_4

product	Q'_H (C.m^{-2})	Q''_H (C.m^{-2})	Q_H (C.m^{-2})	EAS (m^2.g^{-1})
Pt-CH	318.25	533.83	426.04	39.78
Pt-Co-CH	435.28	1024.47	730.87	68.24
Pt-Fe-CH	326.65	756.96	541.81	50.59
Pt-Co-Fe-CH	1131.63	2048.06	1589.84	148.44

first peak is related to the methanol oxidation (I_f) and the second is due to the oxidation of the corresponding intermediates (I_b) produced during the MO reaction.

The characteristics of the CV curves and the corresponding peak potentials (E_p) are in agreement with other works [23, 24]. For MO at GC/PtNPs-CH electrode, I_f was 193.33 mA cm^{-2} and I_b was 153.97 mA cm^{-2}. The I_f/I_b ratio of the electrode for MO was 1.26. Onset potential of MO at GC/PtNPs-CH electrode was 0.199 V.

The first reaction of methanol with Pt nanoparticles is adsorption of methanol on the Pt surface to give Pt(CH_3OH), which requires several free Pt binding sites [25]. Then, dehydrogenation of methanol begins on PtNPs surface. Pt-$(CO)_{ads}$, carbonaceous species such as CO, formaldehyde and formic acid are produced [26]. It is well known that the peak I_f involves the progress of these various steps and depends on the amount of clean active sites available on Pt particles surface. Then, dissociation of water occurs on the pure Pt electrode and the produced OH groups remove the adsorbed CO from the Pt surface [27]. Platinum is oxidized to platinum oxide at more positive potentials. This inhibits the MO reaction but in the backward potential sweep, platinum is produced again by reducing the platinum oxide. MO reaction can occur on the clean platinum surface and I_b appears. I_f/I_b shows the ratio of the amount of methanol oxidized to carbon dioxide to the amount of carbon monoxide [28].

To know the effect of the CoNPs and FeNPs on the electrocatalytical properties of GC/PtNPs-CH electrode, the content of Pt was kept at a constant value (8 mM) and concentration of metal ions as precursor was 0.33 mM. As observed from Fig. 3e and 3f, two peaks of MO can be seen obviously in the range of 0.0 and 1.2 V for GC/PtNPs-FeNPs-CH and GC/PtNPs-CoNPs-CH electrodes. On the GC/PtNPs-FeNPs-CH electrode (Fig. 3e), two oxidation peaks can be seen at 0.841 (E_f) and 0.562 V (E_b). I_f was 251.23 and I_b was 249.70 mA cm^{-2} (I_f/I_b = 1.01). Onset potential of MO at GC/PtNPs-FeNPs-CH was 0.207 V. As seen in Fig. 3f, two oxidation peaks can be obtained obviously at 0.875 (E_f) and 0.596 V (E_b). I_f was 248.66 and I_b was 277.55 mA cm^{-2} (I_f/I_b = 0.89) on the GC/PtNPs-CoNPs-CH electrode. MO reaction on GC/PtNPs-CoNPs-FeNPs-CH electrode was shown in Fig. 3g. As seen, two oxidation peaks

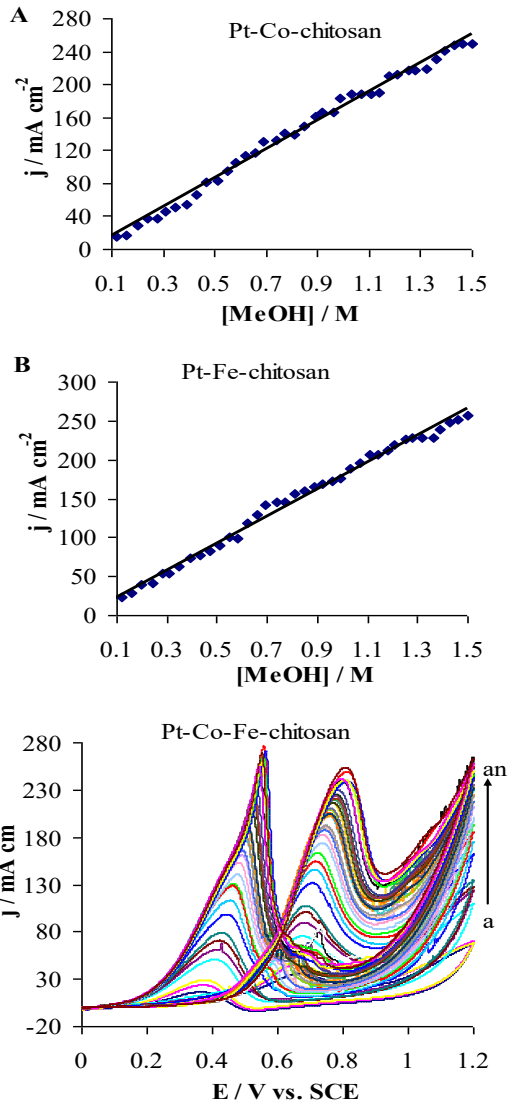

Fig. 4. Cyclic voltammograms for MO on as-prepared electrodes in 0.5 M H2SO4 in different concentration of methanol: a) 0.039, b) 0.079, c) 0.12, d) 0.16, e) 0.2, f) 0.24, g) 0.28, h) 0.31, i) 0.35, j) 0.39, k) 0.43, l) 0.47, m) 0.51, n) 0.55, o) 0.58, p) 0.62, q) 0.66, r) 0.69, s) 0.74, t) 0.77, u) 0.81, v) 0.85, w) 0.89, x) 0.92, y) 0.96, z) 0.99, aa) 1.03, ab) 1.07, ac) 1.11, ad) 1.14, ae) 1.18, af) 1.21, ag) 1.25, ah) 1.28, ai) 1.32, aj) 1.36, ak) 1.39, al) 1.43, am) 1.46, an) 1.50 M.

can be obtained obviously at 0.806 (E_f) and 0.548 V (E_b). I_f/I_b ratio of MO reaction on this electrode was 0.95.

It is obvious that involvement of Co and Fe pointedly increases the activity of modified electrode. The onset potential of a current rise on GC/PtNPs-CH, GC/PtNPs-CoNPs-CH, GC/PtNPs-FeNPs-CH and GC/PtNPs-CoNPs-FeNPs-CH

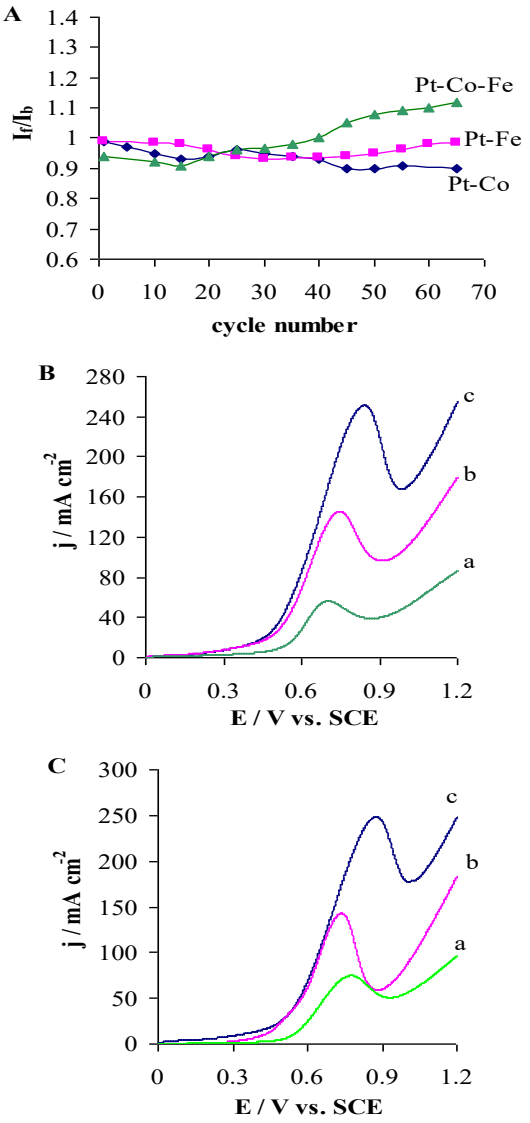

Fig. 5. A) the If/Ib ratio as a function of CV cycle number, B) LSV curves of PtNPs-FeNPs-CH and C) LSV curves of PtNPs-CoNPs-CH nanocomposites at 8 mM of Pt and a: 0.16, b: 0.49 and c: 0.33 mM of Fe and Co nanoparticles

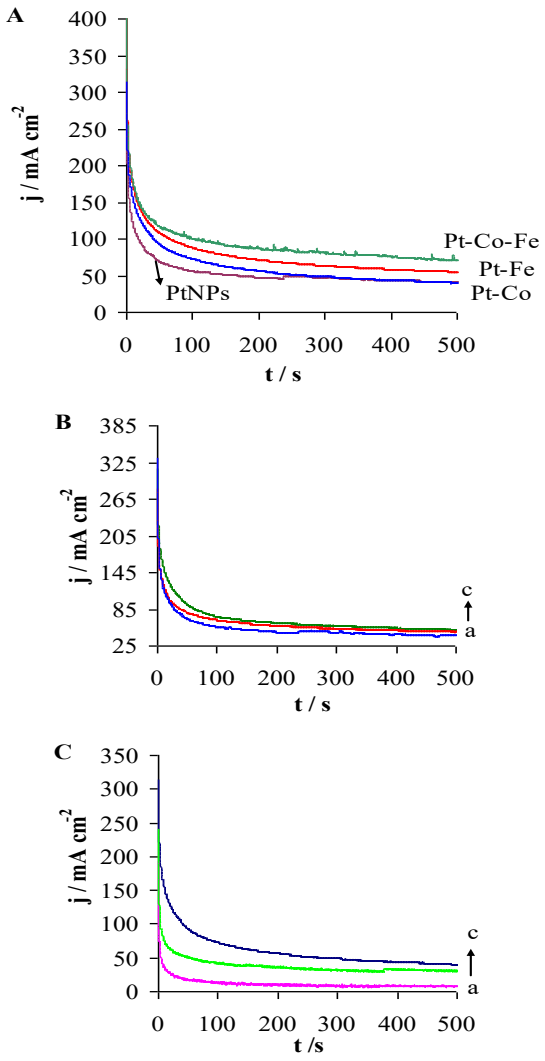

Fig. 6. Chronoamperometry for methanol oxidation at A) all prepared catalysts, B) GC/PtNPs-CoNPs-FeNPs-CH electrocatalyst with 0.33 mM of CoNPs and different concentrations of FeNPs: a) 0.16, b) 0.49, c) 0.33 mM and C) GC/PtNPs-CoNPs-FeNPs-CH electrocatalyst with 0.33 mM of FeNPs and different concentrations of CoNPs: a) 0.16, b) 0.49, c) 0.33 mM in 1.5 M methanol and 0.5 M H_2SO_4

nanocatalysts was 0.199, 0.199, 0.207 and 0.25 V, respectively. The peak current density occurred on GC/PtNPs-CoNPs-CH catalyst (248.66 mA cm^{-2}) was 1.286 times higher than that on GC/PtNPs-CH (193.33 mA cm^{-2}). The peak current density occurred on GC/PtNPs-FeNPs-CH catalyst (251.23 mA cm^{-2}) was 1.299 times higher than that on GC/PtNPs-CH. The peak current density occurred on GC/PtNPs-CoNPs-FeNPs-CH catalyst (253.86 mA cm^{-2}) was 1.313 times higher than that on GC/PtNPs-CH. GC/PtNPs-CoNPs-FeNPs-CH electrode had higher current density than other prepared electrodes for MO reaction. The potential peaks for forward reactions on GC/PtNPs-CH, GC/PtNPs-CoNPs-CH, GC/PtNPs-FeNPs-CH and GC/PtNPs-CoNPs-FeNPs-CH nanocatalysts were 0.767, 0.875, 0.841 and 0.806 respectively. The potential changes were as follows: PtNPs<PtNPs-CoNPs-FeNPs<PtNPs-FeNPs<PtNPs-CoNPs.

As seen, PtNPs-CoNPs-FeNPs-CH catalyst had lower anodic peak potential than PtNPs-CoNPs-CH and PtNPs-FeNPs-CH catalysts indicating that

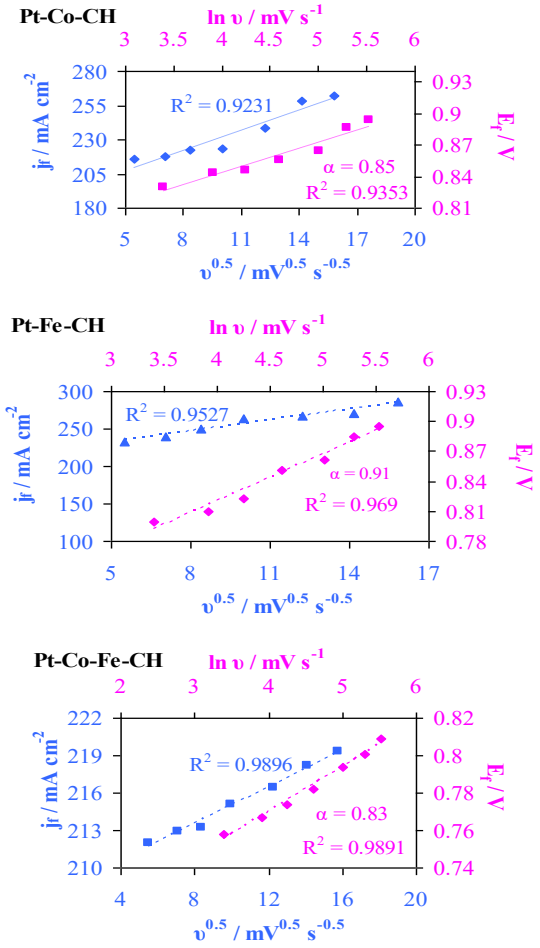

Fig. 7. Anodic current density (jf) vs. square root of scan rate (υ0.5) and irreversibility plot showing peak potential (Ef) vs. ln υ for as-prepared electrodes in 1.5 M methanol and 0.5 M H_2SO_4 at the scan rates of 30, 50, 70, 100, 150, 200 and 250 mV s^{-1}

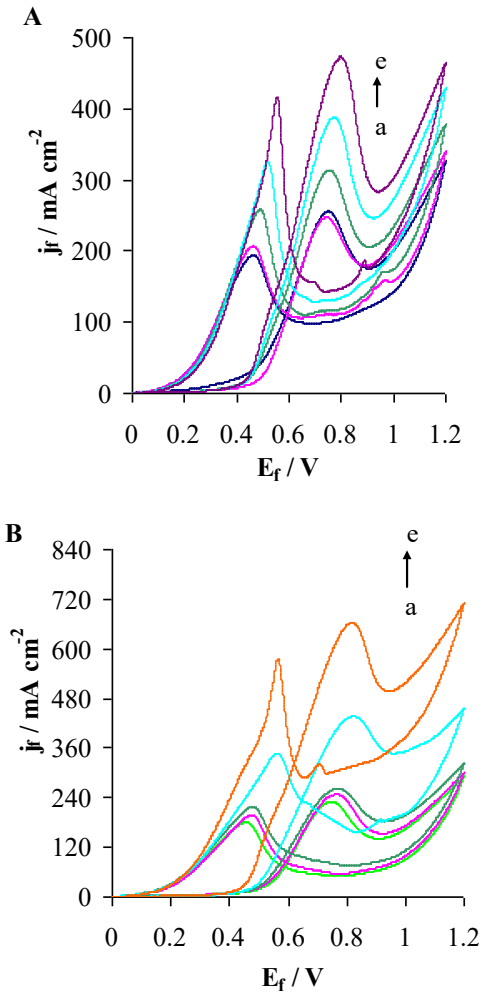

Fig. 8. Cyclic voltammograms of A) PtNPs-FeNPs-CH and B) PtNPs-CoNPs-CH nanocatalysts in different temperatures of a) 20, b) 25, c) 30, d) 35 and e) 40 ˚C

PtNPs-CoNPs-FeNPs-CH nanocomposites had better catalytic activity toward MO reaction.

Also, the potential peaks for backward reaction increased from 0.487 to 0.596 V as follow: PtNPs<PtNPs-CoNPs-FeNPs<PtNPs-FeNPs<PtNPs-CoNPs.

This showed that a certain amount of Fe or Co nanoparticles can improve the electrocatalytic activity of the nanocatalyst for MO reaction in comparison to the pure Pt catalyst. The enhancement of the catalytic activity of binary and ternary catalyst including transition metals beside Pt may be explained through different mechanisms. These mechanisms include the model of oxide formation, the ligand model, the synergistic effect model [29] and bifunctional model [30]. For example, in the ligand model the chemical properties of Pt are changed with the alloying metal and Pt-CO_{ads} bond is weakened. Thus CO poisoning is minimized [31]. In the bifunctional model, dissociation of water at the metal alloy sites creates an oxygenated surface at lower potentials (0.2 V, NHE) compared to monometallic Pt sites. This promotes the oxidation of the adsorbed CO to CO_2, decreases the amount of CO, and thus improves the metal CO tolerance [32]. MO was also investigated on GC/CoNPs-CH (3b) and GC/FeNPs-CH (3c) electrodes without any platinum. As seen in fig. 3b and c, these electrodes did not have any significant activity in MO.

Our results showed that the catalytic activity of MO on GC/PtNPs-CoNPs-FeNPs-CH electrode was

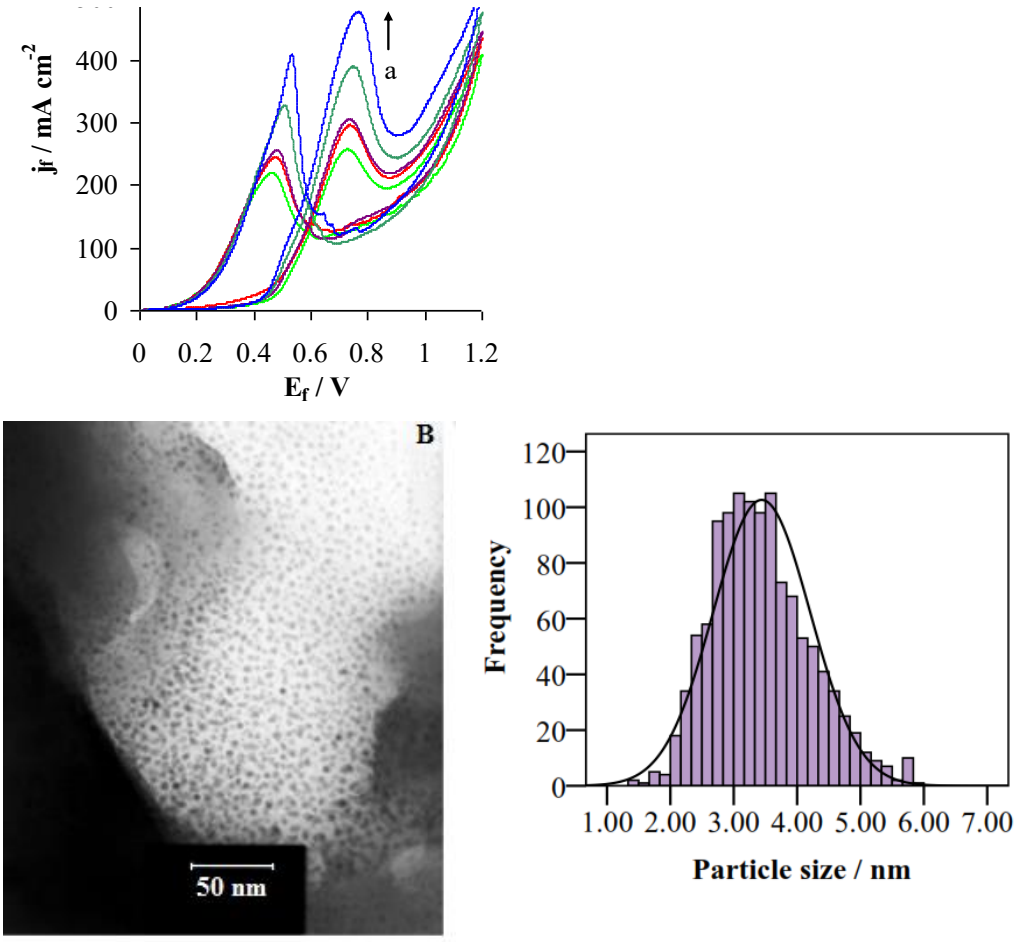

Fig. 9. A) Cyclic voltammograms of PtNPs-CoNPs-FeNPs-CH nanocatalyst in different temperatures of a) 20, b) 25, c) 30, d) 35 and e) 40 ˚C, B) TEM image of Pt-Co-Fe nanoparticles dispersed in chitosan

considerably higher than that obtained at other prepared catalysts due to the lower anodic peak potential and higher current density.

Parameters affecting on electrooxidation of methanol

Our investigations indicated that various parameters such as concentration of methanol, Fe and Co amounts and scan rate were the main factors influencing the performance of all as-prepared electrodes for electrooxidation of methanol. So, these parameters must be optimized.

Fig. 4 showed the effect of methanol concentration on the anodic current density of MO on GC/PtNPs-CoNPs-CH (Fig. 4A) and GC/ PtNPs-FeNPs-CH (Fig. 4B) electrodes. As seen in Fig. 4, the anodic current density increases with increasing methanol concentration and levels off at concentrations higher than 1.5 M. This effect is probably because of the saturation of active sites on the electrode surface. This also shows further that MO at modified electrode is controlled by diffusion process. According to this result, 1.5 M methanol was selected as the optimum concentration.

At GC/PtNPs-CoNPs-CH electrode, when the methanol concentration increases from 0.039 to 1.5 M, the E_f shifts towards positive direction from 0.72 to 0.87 V and at GC/PtNPs-FeNPs-CH electrode, E_f shifts from 0.68 to 0.84 V. This is probably because of the following reason: As the concentration of methanol increases, the poisoning rate of the Pt catalyst will increase thus, the oxidative removal of the strongly adsorbed intermediates will shift to a more positive potential [33]. The effect of methanol concentration was also investigated at GC/PtNPs-CoNPs-FeNPs-CH electrode. The same behavior was observed (Fig. 4C).

In order to examine the poisoning effect of as-prepared electrodes during MO, catalytic activity of PtNPs-CoNPs-CH, PtNPs-FeNPs-CH and PtNPs-CoNPs-FeNPs-CH nanocomposites was investigated through cyclic voltammetry and 65 cycles repeatedly. Fig. 5A showed the I_f/I_b ratios as a function of cycle number. As observed for PtNPs-CoNPs-CH nanocomposite, I_f/I_b decreased during 65 cycles, indicating the poor anti-poisoning performance of this catalyst. For PtNPs-FeNPs-CH, there was a gradual drop of I_f/I_b ratio within the first 30 cycles, whereas the I_f/I_b ratios of PtNPs-FeNPs-CH catalyst exhibited an increasing trend after 30 cycles. For PtNPs-CoNPs-FeNPs-CH catalyst, the I_f/I_b ratio decreased during the first 15 cycles and gradually increased after 15 cycles. PtNPs-CoNPs-FeNPs-CH catalyst had the highest I_f/I_b ratio after 65 cycles, indicating that this catalyst is capable of offering excellent antipoisoning effect toward MO.

The effect of Co and Fe nanoparticle amounts on the catalytic activity of PtNPs-FeNPs-CH and PtNPs-CoNPs-CH nanocatalysts was investigated through LSV under different concentrations of Fe and Co nanoparticles and constant amount of Pt nanoparticles (8mM) (Fig. 5B and 5C). Fig. 5B showed LSV curves of PtNPs-FeNPs-CH nanocomposite with 8mM of Pt nanoparticles and different concentrations 0.16, 0.33 and 0.49 mM of Fe nanoparticles. As seen in Fig. 5B, the best catalytic activity was observed for PtNPs-FeNPs-CH with 8 mM Pt and 0.33 mM Fe nanoparticles. LSV curves of PtNPs-CoNPs-CH nanocatalysts with constant amount (8 mM) of Pt nanoparticles and different concentration (0.16, 0.33 and 0.49 mM) of Co nanoparticles were shown in Fig. 5C.

Similarly, the best catalytic activity was observed for PtNPs-CoNPs-CH with 8 mM Pt and 0.33 mM Co nanoparticles. The effect of Co and Fe nanoparticles on the catalytic activity of GC/PtNPs-CH electrode toward MO was also investigated through chronoamperometry technique.

Chronoamperometry experiments were done at potential value 1 V in 0.5 M H_2SO_4 and 1.5 M methanol (Fig. 6). Fig. 6A showed the chronoamperometry curves of PtNPs-CH, PtNPs-FeNPs-CH, PtNPs-CoNPs-CH and PtNPs-CoNPs-FeNPs-CH nanocomposites with the concentrations of Pt (8 mM), Fe and Co nanoparticles (0.33 mM). As seen in Fig. 6A, all potentiostatic currents decreased rapidly in the

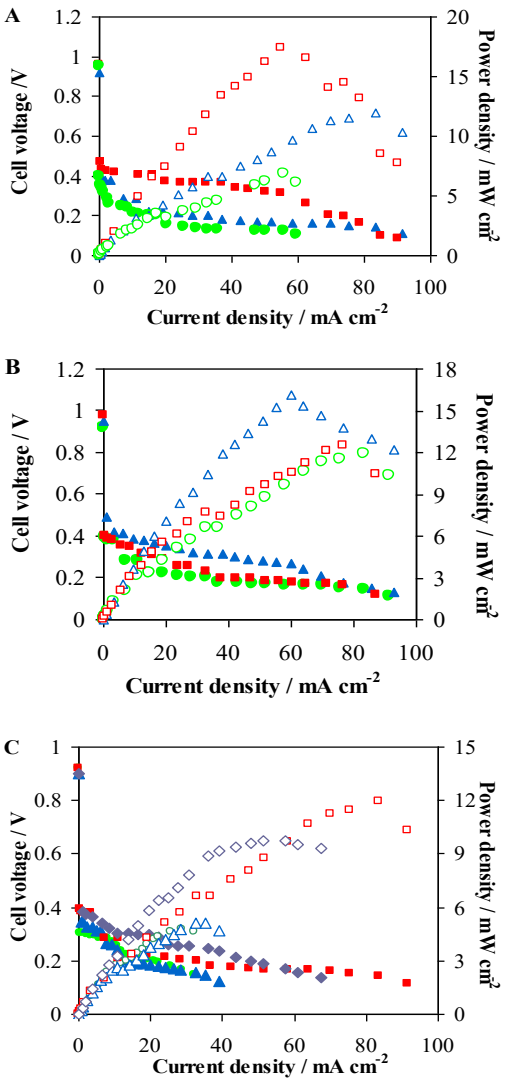

Fig. 10. Electrical performances of a 5 cm^2 DMFC at different (A) temperatures (triangle) 70, (square) 80 and (circle) 90°C ([Methanol]= 1.0 M; [NaOH] = 1.0 M and flow rate = 5 mL min-1), (B) methanol concentrations (circle) 1, (triangle) 2 and (square) 3 M (temperature= 70 °C; [NaOH] = 1.0 M and flow rate = 5 mL min-1) and (C) NaOH concentrations (circle) 0.0, (triangle) 0.5, (square) 1.0, and (diamond) 1.5 M ([Methanol] = 1.0 M; flow rate = 5 mL min-1 and temperature = 70 °C) using the Pt-Co-Fe-CH anode, Pt-CH cathode catalysts and nafion membrane

initial stage. This is attributed to the formation of intermediate species such as CH_3OH_{ads}, CHO_{ads} and CO_{ads} during MO reaction [34]. After a period of 60 s, the current decay became gradual and then remained stable. The SO_4^{2-} anions adsorbed on the bimetallic catalysts surface would restrict MO reaction and cause this time decay [35]. After 200 s, the current density of all the catalysts became

almost constant. The steady-state part of the curve indicated that the stable current of PtNPs-CoNPs-FeNPs-CH electrode was higher than other three catalysts. This result revealed that PtNPs-CoNPs-FeNPs-CH catalyst has the highest stability and the highest electrocatalytic activity toward MO. Thus, PtNPs-CoNPs-FeNPs-CH is a promising catalyst for applications in DMFCs.

Electrocatalytic activity of GC/PtNPs-CoNPs-FeNPs-CH electrode toward methanol electrooxidation was also investigated with different concentration of Fe and Co nanoparticles. In order to investigate the effect of FeNPs concentration, chronoamperometry curves were obtained in the constant amount of Co nanoparticles (0.33 mM) and different concentrations (0.16, 0.33, 0.49 mM) of Fe nanoparticles (Fig. 6B). To determine the effect of Co concentration on the catalytic activity of GC/PtNPs-CoNPs-FeNPs-CH electrode for MO, constant amount of Fe nanoparticles (0.33 mM) and different concentration of CoNPs (0.16, 0.33, 0.49 mM) were used (Fig. 6C). The best result was observed for PtNPs-CoNPs-FeNPs-CH nanocomposite with Pt 8 mM, Co 0.33 mM and Fe 0.33 mM composition.

In order to study the effect of scan rate, the CV curves of PtNPs-CoNPs-CH, PtNPs-FeNPs-CH and PtNPs-CoNPs-FeNPs-CH were obtained at the scan rates of 30, 50, 70, 100, 150, 200 and 250 mV s^{-1}. Based on the CV curves, the anodic peak current densities of MO vs. the square root of the scan rate and the peak potential vs. ln υ have been displayed. The experiments have been done in 1.5 M methanol and 0.5 M H_2SO_4 medium at various scan rates.

It was clear from Fig. 7 that by increasing the scan rate, the anodic peak current density of MO has been increased. The linear relationship (R^2 = 0.92 - 0.99) between the square root of the scan rate and the peak current density demonstrates that MO was diffusion controlled process [36].

As evident from Fig. 7, the peak potential of MO (E_f) amplified with increasing the scan rate, and a linear relationship (R^2 = 0.93 - 0.99) has been obtained between E_f and ln (υ). This shows that the methanol oxidation is an irreversible charge transfer process [37]. The plot of E_p and ln (υ) was a straight line with a slope:

$$\partial E_p/\partial(\ln \upsilon) = R\times T/(1-\alpha) \times n\times F \quad (3)$$

The influence of electrochemical potential on the activation energy of an electrochemical reaction is characterized with α which is the electron transfer coefficient.

The slopes of E_p vs. ln (υ) plots were 29.10, 47.20 and 24.10 mV for GC/PtNPs-CoNPs-CH, GC/PtNPs-FeNPs-CH and GC/PtNPs-CoNPs-FeNPs-CH electrodes, respectively. α value was calculated as 0.85, 0.91 and 0.83 (n = 6 and T = 20 ˚C) for GC/PtNPs-CoNPs-CH, GC/PtNPs-FeNPs-CH and GC/PtNPs-CoNPs-FeNPs-CH electrodes, respectively. This parameter was between 0.5 and 1 for the introduced nanocatalyst showing that MO on the modified electrode has super kinetics.

The effect of temperature on the electrocatalytic activity of PtNPs-CoNPs-CH, PtNPs-FeNPs-CH and PtNPs-CoNPs-FeNPs-CH nanocatalysts toward methanol oxidation was investigated through CV curves obtained in different temperatures ranging from 20 to 40 ˚C. The results were shown in Fig. 8 and 9A. As seen in Fig. 8 and 9A, the anodic current density was increased with increasing of the temperature. In this way, the mass transport is an important factor for higher activity. As indicated for PtNPs-FeNPs-CH nanocatalyst in Fig. 8A, when the temperature changed from 20 to 40 ˚C, the j_f increased from 255.97 to 473.32 mA cm^{-2} with an increment factor of 1.84. For PtNPs-CoNPs-CH nanocatalyst, as the temperature increased from 20 to 40 ˚C, the j_f increased from 230.57 to 663.67 mA cm^{-2} with an increment factor of 2.87 (Fig. 8B).

The effect of temperature on the catalytic activity of PtNPs-CoNPs-FeNPs-CH for methanol electrooxidation was shown in Fig. 9A. As observed in Fig. 9A, when the temperature increased from 20 to 40 ˚C, the j_f increased from 257.66 to 477.57 mA cm^{-2} with an increment factor of 1.85. As seen for all the catalysts, the methanol oxidation activity was enhanced as the temperature increased.

At the same methanol concentration, the higher current density indicated that the fine structure of catalysts possess more available active sites of three metals to participate in the electrochemical reaction. Activation energies were calculated by investigating the MO reaction at different temperatures between 20 and 40 ˚C on GC/PtNPs-FeNPs-CH, GC/PtNPs-CoNPs-CH and GC/PtNPs-CoNPs-FeNPs-CH electrodes.

Activation energies were calculated from the slope of the Arrhenius plots for certain potential values by the use of the Eq. (4):

$$\partial \ln j_p/\partial(1/T) = E_a/R \quad (4)$$

The apparent activation energy of MO at PtNPs-FeNPs-CH, PtNPs-CoNPs-CH and PtNPs-CoNPs-FeNPs-CH electrodes was 11.068, 17.617 and 9.948 kJ mol^{-1}, respectively. Lower activation energy of methanol oxidation at PtNPs-CoNPs-FeNPs-CH electrode indicated that this electrode has better catalytic activity than other prepared catalysts toward methanol oxidation.

TEM image of Pt-Co-Fe nanoparticles dispersed in chitosan was shown in Fig. 9B. These nanoparticles were spherical and their size was around 2 to 5 nm. It was clearly seen that the use of chitosan allows a better dispersion of nanoparticles through larger portion of the surface and thus prevents agglomeration of the metallic particles.

The performance investigation of single cells

The improved performance of the Pt-Co-Fe-CH catalyst as an oxygen storage component was investigated through single cell tests with the MEA made as the anode, and the PtNPs-CH catalyst as the cathode for CH_3OH/O_2. It is known that the efficiency of the electrochemical reaction at the interface between the solid phase of the electrodes (anode and cathode), liquid phase in anode side and gas phase in cathode side determine the performance of the proposed single cell system. Different parameters are effective on the mentioned reaction. We studied the effect of different conditions such as: concentration of methanol solution as fuel, temperature and concentration of NaOH in the carrier stream.

The temperature

In order to determine the effect of temperature on the performance of the fuel cell, different temperatures ranging between 70 - 90 ˚C were tested at a single cell with 5 cm^2 surface area (P_{O2} = 2 bar; [Methanol] = 1 M; flow rate = 5 $ml.min^{-1}$; [NaOH] = 1 M and Nafion® 117 membrane). The Electrical performances (Cell voltage against current density and power density against current density) have been shown in Fig. 10A. The open circuit voltages of the single cells at the various temperatures were 0.92 V at 70 ˚C, 0.96 V at 80 ˚C and 0.95 V at 90 ˚C. The open circuit voltages increased with increasing the temperature. After polarization loss, the potential of single cells were stabled at 0.11 V for 70 ˚C, 0.09 V for 80 ˚C and 0.10 V for 90 ˚C. Also, the observed maximum power densities of single cells were 11.94, 17.38 and 6.82 $mW.cm^{-2}$ at the 70, 80 and 90 ˚C temperatures, respectively. It was observed that increasing of the fuel cell temperature from 70 ˚C to 80 ˚C caused enhancing of the DMFC power density. It is probably because of the faster kinetics of MO and oxygen reduction at the higher temperature. However, increasing of the fuel cell temperature from 80 ˚C to 90 ˚C caused decreasing of its power density. It can be due to the sensitive of membrane-electrode assembly and falling of its performance.

The methanol concentration

The concentration of methanol as a fuel has a significant effect on the electrical performances such as power density and cell voltage, as one would expect. The polarization curves of the single cell system were obtained for different methanol concentrations at a single cell with 5 cm^2 surface area (Temperature = 70 ˚C; P_{O2} = 2 bar; [NaOH] = 1 M; flow rate = 5 $ml.min^{-1}$ and Nafion® 117 membrane). The polarization curves have been showed at Fig. 10B. The open circuit voltages of the single cells were 0.92, 0.95 and 0.98 V for the 1, 2 and 3 M methanol solutions, respectively. The effect of the methanol concentration was the positively and negligibly on the open circuit voltage. After polarization loss, the potential of single cells were stabled at 0.11 V for 1 M, 0.13 V for 2 M and 0.12 V for 3 M methanol solution. The observed maximum power densities of single cells were 11.94, 16.11 and 12.54 $mW\ cm^{-2}$ at the 1, 2 and 3 M methanol solutions, respectively. The power density was enhanced with concentration increasing from 1 M to 2 M of methanol as a fuel that it can be due to the large number and desaturation of the catalytic sites. Then, the electrical performance of the fuel cell was dropped due to the cross-over of methanol and also, the poisoning of anodic and cathodic catalyst.

The NaOH concentration

The potential of using inexpensive metal catalysts and also faster methanol oxidation kinetics in an alkaline solution than acidic media are the main advantages of DMFC [38]. It is known that alkaline electrolytes are better media for performing many catalysts reactions such as oxidation of methanol and reduction of oxygen. It was also shown that MO in alkaline electrolytes is insensitive to the structure, so the use of perovskite-type oxides [39] was investigated in alkaline fuel cells in which the ionic current is because of the conduction of hydroxide ions. These catalysts are significantly cheaper than Pt and Pd based catalysts. The ionic flow in alkaline fuel cells occurs in the reverse direction to that in proton conducting systems. The hydroxide ions

move through the membrane electrolyte along a direction of the electro-osmotic drag opposing methanol flow, thus reducing methanol crossover [40]. The experimental results show that with increasing the pH of the fuel in fuel cells, hydrolysis becomes significant and can compete with the direct reduction reaction of the metal. Reduction of the metal hydroxides produced from hydrolysis can form the metal nanoparticles. Thus, formation of the nanoparticles at high pH is limited by the reduction reactions of various hydroxides and their dissolution rates.

It is known that CO_2 is a byproduct producing from methanol oxidation on the anode side in DMFCs. This byproduct can ruin the anode electrode. This problem can be solved by carbonation of the solution due to CO_2 production in alkaline electrolytes in fuel oxidation route as follow:

$$2\ OH^- + CO_2 \rightarrow CO_3^{2-} + H_2O \quad (5)$$

So, increasing the NaOH concentration decrease the CO_2 fouling. However, with increasing the NaOH concentration in the fuel carrier stream, the carbonate salts are produced and precipitated on the anode electrode [41]. Consequently, this reduces the reactivity for fuel oxidation in the system [42]. Fig. 10C showed the cell performance the different NaOH concentration (P_{O2} = 2 bar; [Methanol] = 1 M; Temperature = 70 ˚C; flow rate = 5 ml.min^{-1} and Nafion® 117 membrane) at a single cell with 5 cm^2 surface area.

The open circuit voltages of the single cells at the various NaOH concentrations were 0.92 V for 0 M, 0.90 V for 0.5 M, 0.92 V for 1 M and 0.90 V for 1.5 M. After polarization loss, the potential of single cells were stabled at 0.15 V for 0 M, 0.12 V for 0.5 M, 0.11 V for 1 M and 0.14 V for 1.5 M of the NaOH concentration in fuel stream. The observed maximum power densities of single cells were 4.72, 5.15, 11.94 and 9.75 mW.cm^{-2} at the 0, 0.5, 1 and 1.5 M of the NaOH concentration in the fuel stream, respectively.

CONCLUSION

In this work, Pt/M-chitosan (M = Co, Fe) nanocomposites dispersed in chitosan polymer were successfully synthesized and characterized. We have investigated the influence of FeNPs and CoNPs in the electrooxidation of methanol in acid media at Pt-chitosan nanocomposite in the temperature range 20-40 ˚C. The GC/PtNPs-CoNPs-CH, GC/PtNPs-FeNPs-CH and GC/PtNPs-CoNPs-FeNPs-CH electrodes were prepared as active electrocatalysts for electrooxidation of methanol. The CV curves and the potentiostatic experiments showed that the catalytic activity of as-prepared catalysts for methanol electrooxidation was increased in the order of PtNPs-CH < PtNPs-CoNPs-CH < PtNPs-FeNPs-CH < PtNPs-CoNPs-FeNPs-CH, in the whole range of temperature. Increasing of the catalytic activity of the catalysts was due to the higher current density, lower anodic peak potential and better antipoisoning effect toward MO obtained after 65 cycles. This result was confirmed with comparing of the electrochemical surface area, the electron transfer coefficient, the activation energy and chronoamperometry result. The apparent activation energies for methanol oxidation reaction were found to be in the order: PtNPs-CoNPs-FeNPs-CH < PtNPs-FeNPs-CH < PtNPs-CoNPs-CH.

ACKNOWLEDGMENT

We thank Esfarayen University of Technology for financial support.

CONFLICT OF INTEREST

The authors declare that there are no conflicts of interest regarding the publication of this manuscript.

REFERENCES

1. Li W, Zhou W, Li H, Zhou Z, Zhou B, Sun G, Xin Q. Nano-stuctured Pt–Fe/C as cathode catalyst in direct methanol fuel cell. Electrochim. Acta. 2004; 49 (7): 1045-1055.
2. Ma X, Luo L, Zhu L, Yu L, Sheng L, An K, Ando Y, Zhao X. Pt-Fe catalyst nanoparticles supported on single-wall carbon nanotubes: Direct synthesis and electrochemical performance for methanol oxidation. J. Power Sources. 2013; 241 (1): 274-280.
3. Reddington E, Sapienza A, Gurau B, Viswanathan R, Sarangapani S, Smotkin ES, Mallouk TE. Combinatorial electrochemistry: A highly parallel, optical screening method for discovery of better electrocatalysts. Science. 1998; 280 (5370): 1735-1737.
4. García-Díaz BL, Colón-Mercado HR, Herrington K, Fox EB. Polarization and Electrocatalyst Selection for Polybenzimidazole Direct Methanol Fuel Cells. J Fuel Cell Sci Technol. 2014; 11 (3): 031001-031005.
5. Barroso de Oliveira M, Profeti LPR, Olivi P. Electrooxidation of methanol on PtMyOx (M=Sn, Mo, Os or W) electrodes. Electrochem. Commun. 2005; 7 (7): 703-709.
6. Hsieh CT, Lin JY. Fabrication of bimetallic Pt–M (M = Fe, Co, and Ni) nanoparticle/carbon nanotube electrocatalysts for direct methanol fuel cells. J. Power Sources. 2009; 188 (2): 347-352.
7. Sankar M, Dimitratos N, Miedziak PJ, Wells PP, Kiely CJ, Hutchings GJ. Designing bimetallic catalysts for a green and sustainable future. hem. Soc. Rev. 2012;41(24):8099-139.
8. Khorasani-Motlagh M, Noroozifar M, Ekrami-Kakhki MS. Investigation of the nanometals (Ni and Sn) in platinum binary and ternary electrocatalysts for methanol electrooxidation. Int. J. Hydrogen Energy. 2011; 36 (18): 11554-11563.

9. Noroozifar M, Khorasani-Motlagh M, Ekrami-Kakhki MS, Khaleghian-Moghadam R. Enhanced electrocatalytic properties of Pt-chitosan nanocomposite for direct methanol fuel cell by $LaFeO_3$ and carbon nanotube. J. Power Sources. 2014; 248 (1): 130-139.
10. Xu D, Bliznakov S, Liu Z, Fang J, Dimitrov N. Composition-dependent electrocatalytic activity of Pt–Cu nanocube catalysts for formic acid oxidation. Angew. Chem. Int. Ed. 2010; 49 (7): 1282-1285.
11. Habibi B, Delnavaz N. Electrosynthesis, characterization and electrocatalytic properties of Pt–Sn/CCE towards oxidation of formic acid. RSC Adv.. 2012; 2 (4): 1609-1617.
12. Salabat A, Barati A, Banijamali N. Synthesis and characterization of the Pt/SiO_2 nanocomposite by the sol-gel method. J Nanostruct. 2011; 1 (1): 1-6.
13. Guo S, Sun S. FePt nanoparticles assembled on graphene as enhanced catalyst for oxygen reduction reaction. J. Am. Ceram. Soc. 2012; 134 (5): 2492-2495.
14. Noroozifar M, Khorasani-Motlagh M, Ekrami-Kakhki MS, Khaleghian-Moghadam R. Electrochemical investigation of Pd nanoparticles and MWCNTs supported Pd nanoparticles-coated electrodes for alcohols (C_1-C_3) oxidation in fuel cells. J. Appl. Electrochem. 2014; 44 (2): 233-243.
15. Guibal E. Heterogeneous catalysis on chitosan-based materials: a review. Prog. Polym. Sci. 2005; 30 (1): 71-109.
16. Huang H, Yuan Q, Yang X. Preparation and characterization of metal-chitosan nanocomposites. Colloids Surf., B. 2004; 39 (1-2): 31-37.
17. Tang Z, Geng D, Lu G. A simple solution-phase reduction method for the synthesis of shape-controlled platinum nanoparticles. Mater. Lett. 2005; 59 (12): 1567-1570.
18. Su YK, Shen CM, Yang TZ, Yang HT, Gao HJ, Li HL. The dependence of Co nanoparticle sizes on the ratio of surfactants and the influence of different crystal sizes on magnetic properties. Appl. Phys. A. 2005; 81 (3): 569-572.
19. Mazumdar H, Haloi N. A study on Biosynthesis of Iron nanoparticles by Pleurotus sp. J Microbiol Biotechnol Res. 2011; 1 (3): 39-49.
20. Rao CV, Singh SK, Viswanathan B. Electrochemical performance of nano-SiC prepared in thermal plasma. Indian J. Chem., Sect A. 2008; 47A (11): 1619-1625.
21. Liu YT, Yuan QB, Duan DH, Zhang ZL, Hao XG, Wei GQ, Liu SB. Electrochemical activity and stability of core-shell Fe_2O_3/Pt nanoparticles for methanol oxidation. J. Power Sources. 2013; 243 (1): 622-629.
22. Kulesza PJ, Matczak M, Wolkiewicz A, Grzybowska B, Galkowski M, Malik MA, Wieckowski A. Electrocatalytic properties of conducting polymer based composite film containing dispersed platinum microparticles towards oxidation of methanol. Electrochim. Acta. 1999; 44 (12): 2131-2137.
23. Ekrami-Kakhki MS, Khorasani-Motlagh M, Noroozifar M. Platinum nanoparticles self-assembled onto chitosan membrane as anode for direct methanol fuel cell. J. Appl. Electrochem. 2011; 41 (5): 527-534.
24. Yavari Z, Noroozifar M, Khorasani-Motlagh M. Multifunctional catalysts toward methanol oxidation in direct methanol fuel cell. J. Appl. Electrochem. 2015; 45 (5): 439-451.
25. Iwasita T. Electrocatalysis of methanol oxidation. Electrochim. Acta . 2002; 47 (22-23): 3663-3674.
26. Korzeniewski C, Childers CL. Formaldehyde yields from methanol electrochemical oxidation on platinum. J. Phys. Chem. B. 1998; 102 (3): 489-492.
27. Leger JM. Preparation and activity of mono- or bi-metallic nanoparticles for electrocatalytic reactions. Electrochim. Acta. 2005; 50 (15): 3123-3129.
28. Pournaghi-Azar MH, Habibi B. Electrocatalytic oxidation of methanol on poly (phenylenediamines) film palladized aluminum electrodes, modified by Pt micro-particles: comparison of permselectivity of the films for methanol. J. Electroanal. Chem. 2007; 601 (1-2): 53-62.
29. Lim DH, Lee WD, Lee HI. Highly dispersed and nano-sized Pt-based electrocatalysts for low-temperature fuel cells. Catal. Surv. Asia. 2008; 12 (4): 310-325.
30. Park KW, Choi JH, Kwon BK, Lee SA, Sung YE, Ha HY, Hong SA, Kim H, Wieckowski A. Chemical and electronic effects of Ni in Pt/Ni and Pt/Ru/Ni alloy nanoparticles in methanol electrooxidation. J. Phys. Chem. B. 2002; 106 (8): 1869-1877.
31. Antolini E. Formation of carbon-supported PtM alloys for low temperature fuel cells: a review. Mater. Chem. Phys. . 2003; 78 (3): 563-573.
32. Yajima T, Wakabayashi N, Uchida H, Watanabe M. Adsorbed water for the electro-oxidation of methanol at Pt-Ru alloy. Chem. Commun. 2003; 7 (1): 828-829.
33. He Z, Chen J, Liu D, Zhou H, Kuang Y. Electrodeposition of Pt-Ru nanoparticles on carbon nanotubes and their electrocatalytic properties for methanol electrooxidation. Diamond Relat. Mater. 2004; 13 (10): 1764-1770.
34. Kabbabi A, Faure R, Durand R, Beden B, Hahn F, Leger JM, Lamy C. In situ FTIRS study of the electrocatalytic oxidation of carbon monoxide and methanol at platinum–ruthenium bulk alloy. J. Electroanal. Chem. 1998; 444 (1): 41-53.
35. Jiang J, Kucernak A. Electrooxidation of small organic molecules on mesoporous precious metal catalysts: II: CO and methanol on platinum–ruthenium alloy. J. Electroanal. Chem. 2003; 543 (2): 187-199.
36. Zhao Y, Wang R, Han Z, Li C, Wang Y, Chi B, Li J, Wang X. Electrooxidation of methanol and ethanol in acidic medium using a platinum electrode modified with lanthanum-doped tantalum oxide film. Electrochim. Acta. 2015; 151 (1): 544-551.
37. Guo DJ, Li HL. Electrocatalytic oxidation of methanol on Pt modified single- walled carbon nanotubes. J. Power Sources. 2006; 160 (1): 44-49.
38. Kim J, Momma T, Osaka T. Cell performance of Pd–Sn catalyst in passive direct methanol alkaline fuel cell using anion exchange membrane. J. Power Sources. 2009; 189 (2): 999-1002.
39. Miyazaki K, Sugimura N, Matsuoka K, Iriyama Y, Abe T, Matsuoka M, Ogumi Z. Perovskite-type oxides $La_{1-x}Sr_xMnO_3$ for cathode catalysts in direct ethylene glycol alkaline fuel cells. J. Power Sources. 2008; 178 (2): 683-686.
40. Yu EH, Scott K. Direct methanol alkaline fuel cell with catalysed metal mesh anodes. Electrochem. Commun. 2004; 6 (4): 361-365.
4. Gulzow E. Alkaline fuel cells: a critical view. J. Power Sources. 1996; 61 (1-2): 99-104.
42. Wang Y, Li L, Hu L, Zhuang L, Lu J, Xu B. A feasibility analysis for alkaline membrane direct methanol fuel cell: thermodynamic disadvantages versus kinetic advantages. Electrochem. Commun. 2003; 5 (8): 662-666.